Pure Appl. Chem., Vol. 84, No. 12, pp. 2507–2520, 2012.
http://dx.doi.org/10.1351/PAC-CON-11-12-02

Role of nanosized oxide in catalysis on the nanoporous surface of zeolite particles*

Toshiyuki Kimura[1], Chen Liu[2], Xiaohong Li[1], and Sachio Asaoka[1,‡]

[1]School of Environmental Engineering, The University of Kitakyushu, 1-1 Hibikino, Wakamatsu, Kitakyushu, 808-0135, Japan; [2]Environmental Geochemistry, China University of Geosciences, 29 Xueyuan Lu, Beijing, 100083, China

Abstract: Based on our studies on the hybrid catalysts of nanosized (***ns***) oxide with zeolite, products obtained from the isomerization and hydrocracking of heavier *n*-paraffins and the role of ***ns*** oxide were investigated using a tricomponent catalyst of [Ni-Mo/γ-Al_2O_3], ***ns*** oxide, and H-beta zeolite catalyst, which showed high activity, high isomerization selectivity, and mild cracking ability. A concerted effect of the three components was observed. From the observed hybridization state of the catalyst, it was suggested that the concerted effect was obtained because the components become attached to each other. The individual and concerted effects of each component and two components, respectively, were investigated based on the ratio of [Ni-Mo/γ-Al_2O_3]/[H-beta zeolite], the content of ***ns*** oxide, the amount of metal, the type of ***ns*** oxide species, and the reduction state of metal. It was confirmed that in order to obtain the highest concerted effect, the ratios of [Ni-Mo/γ-Al_2O_3]/[H-beta zeolite] and/or ***ns*** oxide/zeolite are important. Furthermore, among the ***ns*** oxide species, ***ns***Al_2O_3-***ns***TiO_2 displayed the highest activity and cracking ability with an over-cracking suppression. In addition to increasing the concerted effect in the tricomponent catalyst, the performance of this catalyst could also be further increased by controlling the amount and reduction state of metal.

Keywords: catalysis; nanocomposites; nanoparticles; nanostructured materials; zeolites.

INTRODUCTION

Gasoline has recently been produced via reformation of naphtha and/or fluidized-bed catalytic cracking of hydrotreated vacuum gas oil. The oil produced by these processes contains a large amount of aromatic and olefin components that confer a high octane value. However, recently fuel quality regulations reduced the levels of aromatics and olefin that are permissible. Consequently, an efficient catalyst is desired to obtain lighter isoparaffins from heavy normal paraffins by isomerization and hydrocracking, producing high-octane gasoline.

Catalysts that have been developed for hydrocracking can be broadly grouped into two categories; amorphous (i.e., non-crystalline) and zeolitic (i.e., crystalline). Amorphous catalysts are composite oxides made from amorphous substances, such as silica-alumina, alumina, and silica-titania, which exhibit solid acidity and have a controlled pore structure. Mild hydrocracking activities can be achieved by adding a non-zeolitic promoter, such as boron, or supporting metals, such as Ni–Mo (hereafter,

Pure Appl. Chem.* **84, 2499–2675 (2012). A collection of invited papers based on presentations at the 7th International Conference on Novel Materials and their Synthesis (NMS-VII) and the 21st International Symposium on Fine Chemistry and Functional Polymers (FCFP-XXI), Shanghai, China, 16–21 October 2011.
‡Corresponding author: E-mail: asaoka@kitakyu-u.ac.jp

referred to as NiMo) [1–3]. The hydrocracking activity of amorphous catalysts in cracking and isomerization can be enhanced by incorporating a strong non-zeolitic acid, such as heteropolyacids, tungstasulfate, and zirconia [4–7]. Hydrogenation and dehydrogenation can be achieved and modified by using noble metals, such as Pt and Pd [8–13]. On the other hand, zeolitic catalysts have H-type zeolite as a solid acid. They have high cracking ability since they have a high degree of acidity and can achieve higher activity than amorphous catalysts without any enhancement. The hydrogenation and dehydrogenation functions of zeolite catalysts are imparted and modified by NiMo or noble metals, such as Pt and Pd [14–21]. Some hybrid catalysts that are a mixture of amorphous and zeolitic catalysts have been developed [22–24]. Furthermore, the mechanism of hydrocracking and isomerization of *n*-hexadecane has been investigated [25–27].

Zeolitic catalysts containing various sub-nanometer pores and unimodal nanoporous oxides with pore sizes ranging from about 1 nm to several tens of nanometers have been the focus of our recent research. This research has resulted in design advances of a catalyst for various industrial applications, including hydrodesulfurization [28,29], N_2O decomposition [30], hydrocracking [31–34], skeletal isomerization [35,36], cracking–reforming [37], and catalytic cracking [38–40]. As efficient hydrocracking catalysts, hydro-reform catalysts that have high selectivity for producing lower isoparaffins from higher *n*-paraffin were studied to obtain environmentally friendly gasoline [31–34]. The catalytic performance of these catalysts in converting *n*-hexadecane (n-$C_{16}H_{34}$) into isoparaffins with carbon numbers ranging from 5 to 13 was studied. Tricomponent nanoporous and nanosized (***ns***) catalysts composed of Pt/γ-Al_2O_3 or NiMo/γ-Al_2O_3, ***ns*** oxide, and crystalline zeolite (several tens of nanometers in size) had relatively high activities and selectivities due to the concerted effects between Pt/γ-Al_2O_3 or NiMo/γ-Al_2O_3, the ***ns*** oxide and zeolite composite.

The Pt/γ-Al_2O_3 content of the tricomponent catalyst, which is responsible for the hydrogenation and skeletal isomerization activities, enhances the cracking activity of the ***ns***Al_2O_3/H-beta zeolite composite. Moreover, ***ns***Al_2O_3/H-beta zeolite catalyst with Pt directly supported on it can have higher activity than [Pt/γ-Al_2O_3]/***ns***Al_2O_3/H-beta zeolite catalyst due to the close proximity between Pt and zeolite compared to Pt/γ-Al_2O_3. Meanwhile, nanoporous catalyst is produced by the addition of the ***ns***Al_2O_3 component, resulting in high conversion and high isoselectivity of large-molecule reactants on the catalyst. In addition, the catalytic performance is appropriate for the enhanced production of isoparaffins for gasoline.

On the other hand, the NiMo/γ-Al_2O_3 content of the tricomponent catalyst, which is responsible for the skeletal isomerization activity, enhances the cracking activity of the ***ns***Al_2O_3/ultrastable Y (USY) zeolite composite, yielding isoparaffins with carbon numbers ranging from 6 to 12 since the cracking follows after the isomerization of *n*-hexadecane. A catalyst composed of USY zeolite (molar ratio of SiO_2/Al_2O_3 = 12) could be activated by ***ns***Al_2O_3. The catalytic properties of the tricomponent catalyst partially depend on the active sites that form at the boundary between ***ns*** oxides and zeolite. These active sites play a major role as mild-moderate and mild-strong acids during isomerization and cracking. They are generated when Si–OH in the nanopores of USY zeolite, produced by dealumination, traps Al–OH in the ***ns***Al_2O_3 precursor. On the other hand, we have found that catalysts composed of beta zeolite are activated more by ***ns***SiO_2 than ***ns***Al_2O_3 and that they have higher activities than a catalyst composed of USY zeolite [32]. Tricomponent catalysts composed of NiMo/γ-Al_2O_3, ***ns*** oxide, and H-beta zeolite were investigated as a more efficient hydrocracking and isomerization catalytic system for producing isoparaffins. Their catalytic performance depends on the state of the zeolite; beta zeolite with ***ns***Al_2O_3 is more active than beta zeolite with ***ns***SiO_2. Catalysts containing dealuminated beta zeolite with ***ns***Al_2O_3 have high activity and iso-selectivity; their catalytic performances are suitable for the production of isoparaffins for the gasoline fraction. The concerted effect between NiMo/γ-Al_2O_3, ***ns*** oxide, and beta zeolite on the catalysis of hydrocracking and isomerization of heavier paraffins was also investigated. The catalytic performance of a tricomponent catalyst consisting of beta zeolite, ***ns***Al_2O_3, and NiMo/γAl_2O_3 depends on the state of zeolite. A higher SiO_2/Al_2O_3 ratio of zeolite enhances the cracking activity of the catalyst. Since acid treatment removes unstable aluminum

from the surface of beta zeolite, the SiO_2/Al_2O_3 ratio of the surface increases; in contrast, the SiO_2/Al_2O_3 ratio of the framework remains almost constant. Catalysts containing dealuminated beta zeolite have high cracking activity on their surfaces and retain high isomerization activity. Catalysts containing dealuminated beta zeolite with ***ns***Al_2O_3 have high activity and isoselectivity; their catalytic performances are suitable for the production of isoparaffins for the gasoline fraction [34]. The effect of metal and ***ns*** oxide in a tricomponent catalyst consisting of beta zeolite, ***ns***Al_2O_3, and NiMo/γ-Al_2O_3 was also investigated.

EXPERIMENTAL

Catalyst preparation

The NiMo/γ-Al_2O_3 catalyst (Ni: 6.2 wt %, Mo: 10.3 wt %) was prepared by co-impregnation using the incipient wetness method. The catalyst was loaded with 0.39 g/g-(γ-Al_2O_3) and 0.36 g/g-(γ-Al_2O_3) of $Ni(NO_3)_2$ $6H_2O$ and $(NH_4)_6Mo_7O_{24}$ $4H_2O$, respectively in the following manner. A laboratory-produced Al_2O_3 extrudate with 11 nm unimodal pores, and a high surface area of 225 m^2/g was used as the metal carrier. 100 g of the alumina extrudate was impregnated with a NiMo metal solution. A solution of 39 g of nickel nitrate hexahydrate [$Ni(NO_3)_2$ $6H_2O$] was prepared in 40 ml of water. Similarly, 26 g of hexaammonium heptamolybdate tetrahydrate [$(NH_4)_6Mo_7O_{24}$ $4H_2O$] was dissolved in 40 ml of water and heated at 40~50 °C to dissolve the solid. The two solutions were mixed and quickly added to the extrudates. They were then mixed well to ensure that the alumina was homogeneously impregnated by the solution. The mixing and impregnation were performed quickly to avoid complex formation between the two solutions. The impregnated extrudate was aged overnight in a sealed container at room temperature. It was then dried at 120 °C for 5 h and calcined at 550 °C for 2 h. A metal-impregnated alumina (NiMo/γ-Al_2O_3) powder (particle size: 100 μm) was obtained by grinding the catalyst.

Cataloid AP-1 (JGC Catalyst and Chemical Industry Co.) was used as the ***ns*** alumina precursor. It consists of 71.0 wt % alumina, 11.0 wt % acetic acid, and 18.0 wt % water and has an average crystalline size of 5.4 nm. For comparison with ***ns***Al_2O_3, an ***ns*** silica gel (Aerosil 200, Japan Aerosil Co.) was used as ***ns***SiO_2. It has an average primary particle size of ca. 12 nm. In addition, ***ns*** titania gel (laboratory prepared by precipitation) was used as an ***ns***TiO_2 precursor that has an average primary particle size of ca. 10 nm. Beta zeolites were synthesized from the parent gels with different compositions using tetraethyl ammonium hydroxide as a structure-directing agent at 165 °C. These zeolite powders were converted into H-type zeolites by conventional ion exchange with an aqueous solution of NH_4Cl. The beta zeolite has a SiO_2/Al_2O_3 molar ratio of 25 and a crystalline size of ca. 40 nm.

[NiMo/γ-Al_2O_3]/***ns*** oxide/H-beta zeolite catalysts were synthesized by wet mixing followed by calcination. Three of these solid powders were mixed with water to form a thick paste, and this paste was mechanically kneaded. After kneading, the catalysts were extruded into pellets. They were then dried by leaving overnight at room temperature and heating at 120 °C for 3 h. Finally, they were calcinated at 550 °C for 3 h.

The di- and tricomponent catalysts were made from ***ns*** oxide and beta zeolite (typically a dry weight ratio of 1:2) and from NiMo/γ-Al_2O_3, ***ns*** oxide, and beta zeolite (typically a dry weight ratio of 2:1:2), respectively.

Reaction tests and catalyst evaluation

The catalytic performances of the catalysts were evaluated using a feedstock of *n*-hexadecane (*n*-$C_{16}H_{34}$), which has a normal boiling point of 287 °C. This compound was selected as a model of paraffin that contains gas and heavy oils. The light gas oil and the vacuum gas oil had boiling points in the range 232~566 °C. *n*-Hexadecane being the heaviest *n*-paraffin is easy to handle since it is a liquid at room temperature and is difficult to crack. A continuous-flow reactor with a fixed-bed catalyst vol-

ume of 0.5 ml was used for the reaction tests at a temperature of 275 °C under hydrogen pressure. The typical reaction conditions were: liquid hourly space velocity (LHSV): 4.1 h^{-1}; pressure: 0.12 MPa; $C_{16}H_{34}/H_2$ molar ratio; 1:15. Prior to the reaction test, the catalysts were reduced by a H_2 flow [gaseous hourly space velocity (GHSV): 5000 h^{-1}; reduction temperature: 450 °C; reduction time: 3 h].

Catalyst characterization

Elemental compositions of the catalyst surface layer were determined by X-ray photoelectron spectroscopy (XPS). XPS was done by using a KRATOS spectrometer equipped with a mono Al source operating at 450 W. The spectra of the samples were acquired at narrow scans with a rather high 40 eV pass energy at room temperature. The spectrometer energy scale was calibrated with Ag 3d5/2. The binding energies and atomic concentrations of the catalysts were calculated using the XPS results by the total integrated peak areas of the Al 2p, Si 2p, Ni 2p2/3, Mo 3d5/2, O 1s, and C 1s regions.

RESULT AND DISCUSSION

Ratio of Ni-Mo/γ-Al_2O_3 to H-beta zeolite in a tricomponent catalyst

For a typical tricomponent catalyst consisting of a ratio of [Ni-Mo/γ-Al_2O_3] (hereafter, referred to as the metal catalysts)/***ns***Al_2O_3/H-beta zeolite of 2:1:2, we varied the metal catalyst/H-beta zeolite ratio at 0.33, 1, 2, and 3 to investigate the effects on the reaction performance. The results are shown in Figs. 1 and 2.

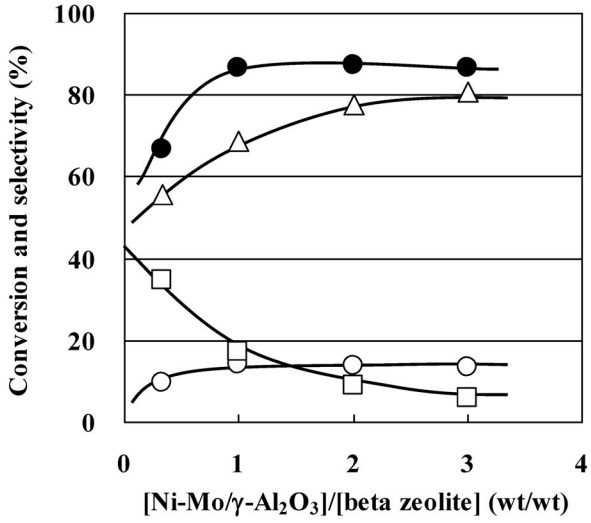

Fig. 1 Conversion and selectivity depending on the [NiMo/γ-Al_2O_3]/[H-beta zeolite] ratio. ●: conversion; ○: normal paraffins; △: isoparaffins; □: olefins.

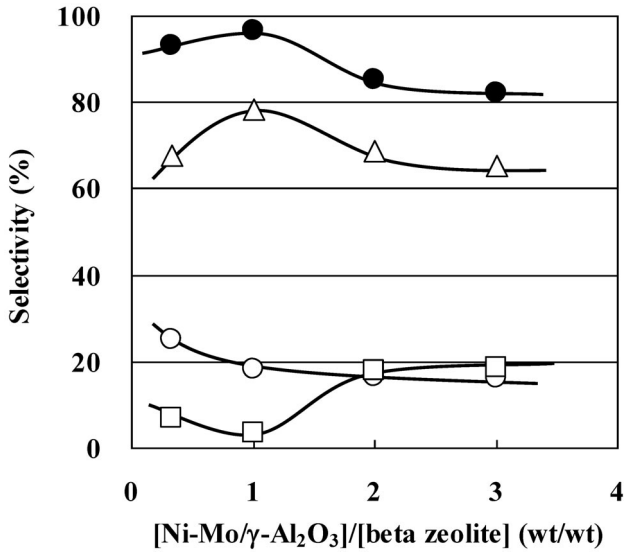

Fig. 2 Selectivity of carbon number depending on the [NiMo/γ-Al_2O_3]/[H-beta zeolite] ratio. ●: cracking selectivity; ○: C_3–C_4 hydrocarbons; △: C_5–C_{13} hydrocarbons; □: C_{16} hydrocarbons.

As shown in Fig. 1, not only the activity increased with increase of the ratio of metal catalysts/zeolite to 1.0, but isoparaffin selectivity also increased, while olefin selectivity decreased. As shown in Fig. 2, the tricomponent catalyst had the highest selectivity for cracking and mild-cracking (C_5~C_{13}) at a metal catalysts/H-beta zeolite ratio at 1.0. Furthermore, over-cracking was suppressed at the ratio. Generally, the cracking reaction needs a certain amount of zeolite, however, in the tricomponent catalyst, it was confirmed that even a small amount is enough for a cracking reaction. In our previous research, it was found that the generation of acid site at the boundary between zeolite and ***ns***Al_2O_3 by hybridization of zeolite and ***ns***Al_2O_3 [31–40]. Formation of the tricomponent catalyst with mild-moderate and mild-strong acid sites at the boundary between ***ns***Al_2O_3 and zeolite can be obtained. It is considered that these acid sites have milder cracking ability than zeolite acid sites. Therefore, the activity of the tricomponent catalyst could be maintained despite the decreased in the ratio of zeolite. It is clarified that a balanced composition of metal catalyst, H-beta zeolite, ***ns***Al_2O_3 is important for high performance of the tricomponent catalyst.

Catalytic performance depending on the *ns*Al_2O_3 content

The effect of ***ns***Al_2O_3 content in the tricomponent catalyst was investigated. As mentioned above, ***ns***Al_2O_3 has mild cracking ability by forming mild-moderate and mild-strong acid sites at the boundary between ***ns***Al_2O_3 and zeolite. Therefore, it was supposed that the content of ***ns***Al_2O_3 should affect the activity and over-cracked products (C_3~C_4). The results are shown in Figs. 3–5.

As shown in Fig. 3, instead of observing increasing olefin selectivity, isoparaffin and *n*-paraffin selectivity decreased due to the decreased Ni and Mo amount per catalyst weight. The *n*-hexadecane conversion increased to a ***ns***Al_2O_3 content of 20 wt %, and then, rapidly decreased. As shown in Fig. 4, when the ***ns***Al_2O_3 content is 20 wt %, the selectivity of cracking and mild cracking is the highest. Figure 5 shows the relative activity per zeolite on this catalyst at the different ***ns***Al_2O_3 contents. It was confirmed that the tricomponent catalyst has an activity per zeolite of 1.4 times higher compared to the dicomponent catalyst when the ***ns***Al_2O_3 content is 20 wt %. It is considered that in addition to the zeolite acid sites, other acid sites, which have mild cracking ability, were formed at the boundary

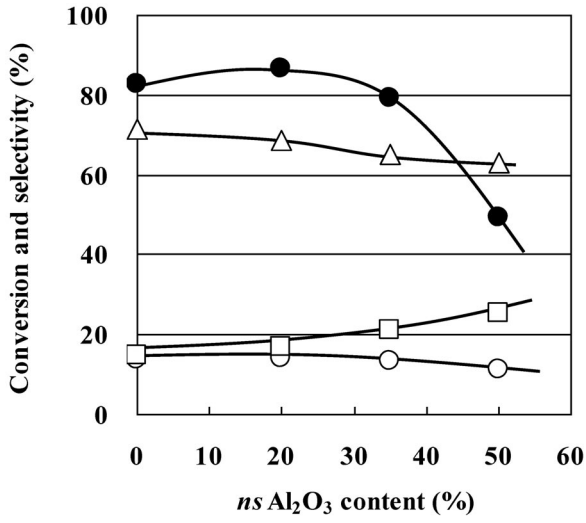

Fig. 3 Conversion and selectivity depending on the ***ns***Al_2O_3 content. ●: conversion; ○: normal paraffins; △: isoparaffins; □: olefins.

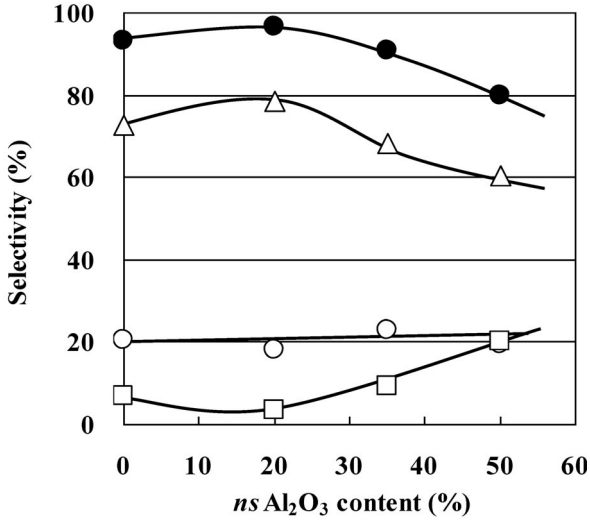

Fig. 4 Selectivity of carbon number depending on the ***ns***Al_2O_3 content. ●: cracking selectivity; ○: C_3–C_4 hydrocarbons; △: C_5–C_{13} hydrocarbons; □: C_{16} hydrocarbons.

between ***ns***Al_2O_3 and zeolite, and the amount of the acid sites depends on the contact area per catalyst between ***ns***Al_2O_3 and zeolite. Therefore, the contact area of ***ns***Al_2O_3 and zeolite is the largest when the ***ns***Al_2O_3 content is 20 wt %, in which the tricomponent catalyst had the highest activity and mild cracking activity.

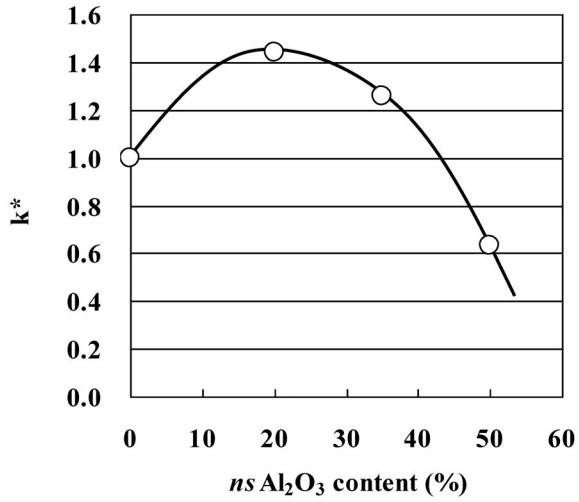

Fig. 5 Relative activity per zeolite weight in the tricomponent catalyst.

Catalytic performance depending on the amount of supported Ni and Mo

The effect of Ni amount in the tricomponent catalyst on the catalytic performance was investigated. Figures 6 and 7 show the effect of Ni amount which are examined from 0 to 5 wt % with a constant Mo amount of 4.1 wt %. Similar to Fig. 1, not only the activity increased with increasing amount of Ni, but isoparaffin selectivity also increased, while olefin selectivity decreased. It is shown that the hydrogenation ability with Ni can be achieved at a certain amount. As shown in Fig. 7, the cracking ability and mild cracking ability are the highest at 2.5 wt % Ni loading amount. Further increase in the Ni amount causes over-cracking.

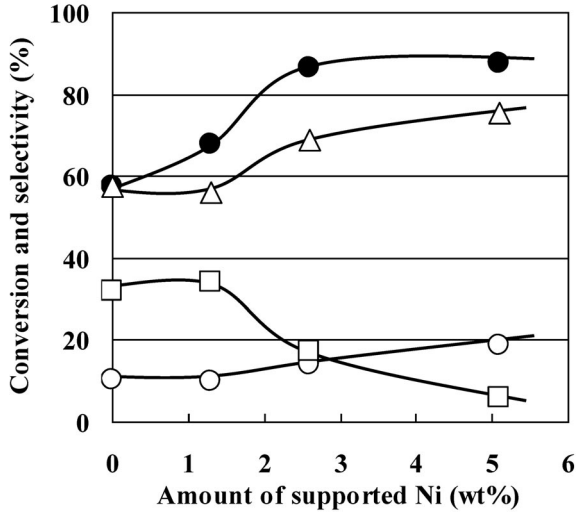

Fig. 6 Conversion and selectivity depending on the amount of supported Ni. ●: conversion; ○: normal paraffins; △: isoparaffins; □: olefins.

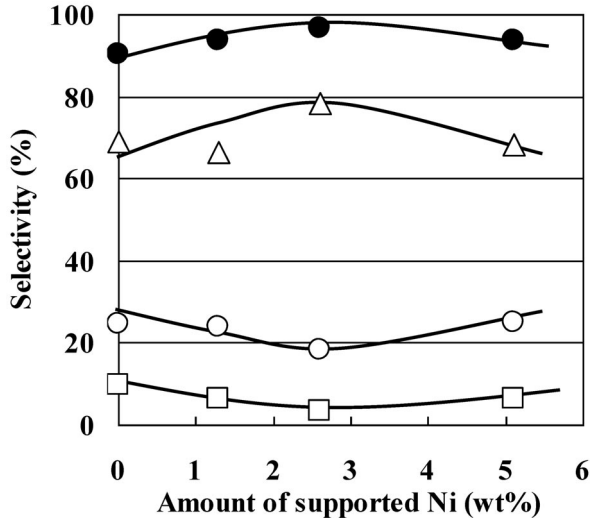

Fig. 7 Selectivity of carbon number depending on the amount of supported Ni. ●: cracking selectivity; ○: C_3–C_4 hydrocarbons; △: C_5–C_{13} hydrocarbons; □: C_{16} hydrocarbons.

The effect of Mo amount on the catalytic performance was investigated. Figures 8 and 9 show the effect of Mo amount, which are examined from 0 to 5.5 wt % with a constant Ni amount of 2.6 wt %. As shown in Fig. 8, not only the activity increased with increasing amount of Mo, but isoparaffin selectivity also increased since the Mo/γ-Al_2O_3 catalyst has isomerization ability [42]. On the other hand, olefin selectivity has rapidly increased with the Mo amount of more than 5 wt %. It is considered that insufficient reduction of NiO is due to the supply of oxygen from over-supported MoO_3.

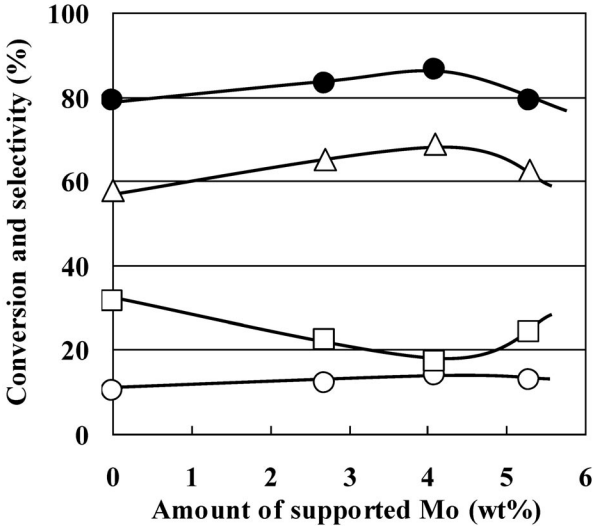

Fig. 8 Conversion and selectivity depending on the amount of supported Mo. ●: conversion; ○: normal paraffins; △: isoparaffins; □: olefins.

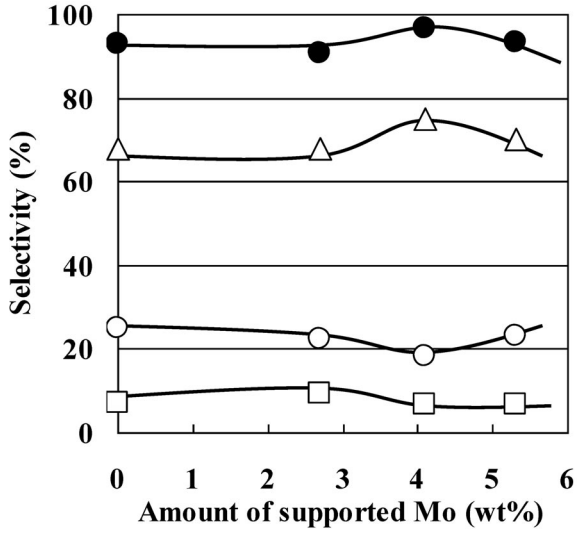

Fig. 9 Selectivity of carbon number depending on the amount of supported Mo. ●: cracking selectivity; ○: C_3–C_4 hydrocarbons; △: C_5–C_{13} hydrocarbons; □: C_{16} hydrocarbons.

Effect of *ns* oxide species and mixture ratio of *ns* oxide

The individual effect of each ***ns***SiO_2, ***ns***Al_2O_3, and ***ns***TiO_2 and the hybridization effect of the composites were investigated. Table 1 shows the comparison for catalysts consisting of each mono ***ns*** oxide; ***ns***SiO_2 gave mild cracking fraction, ***ns***Al_2O_3 gave mild cracking and heavier fraction than ***ns***SiO_2, and ***ns***TiO_2 gave over-cracking and heavier fraction that remained. Therefore, the concerted effect between ***ns***Al_2O_3 and H-beta is the most effective among the mono ***ns*** oxides. The activity of the acid sites at the boundary between ***ns***Al_2O_3 and H-beta zeolite could be increased, and the over-cracking reaction could be suppressed. ***ns***SiO_2-***ns***Al_2O_3, ***ns***SiO_2-***ns***TiO_2, ***ns***Al_2O_3-***ns***TiO_2, and ***ns***SiO_2-***ns***Al_2O_3-***ns***TiO_2 were selected as multi ***ns*** oxides. Table 2 shows the comparison for catalysts consisting of the multi ***ns*** oxides. ***ns***Al_2O_3-***ns***TiO_2 had the highest activity and cracking with an over-cracking suppression considered to be due to the individual and concerted effects of ***ns***Al_2O_3 and ***ns***TiO_2. Accordingly, the mixture ratio of ***ns***Al_2O_3/***ns***TiO_2 in the tricomponent catalyst was investigated. Figure 10 shows that the highest activity was obtained at a 50/50 ratio of ***ns***Al_2O_3/***ns***TiO_2. The acid sites formed by ***ns***Al_2O_3-***ns***TiO_2 composite and the boundary between ***ns***Al_2O_3 and H-beta zeolite provide effective isomerization of *n*-hexadecane.

Table 1 Effect of mono ***ns*** oxide species.

ns Oxide	None	***ns*** SiO_2	***ns*** Al_2O_3	***ns*** TiO_2
Conversion (%)	82.8	86.1	86.6	85.6
Cracked sel. (%)	93.1	96.9	96.7	93.5
Isoparaffin sel. (%)	71.3	70.2	68.7	72.1
Olefin sel. (%)	14.7	14.9	17.1	13.1
C_3~C_4 sel. (%)	20.4	17.3	18.3	20.8
C_5~C_{13} sel. (%)	72.7	79.6	78.4	72.5
C_{16} sel. (%)	6.9	3.1	3.3	6.7

Table 2 Effect of multi ***ns*** oxide species.

ns Oxide	***ns***SiO_2-***ns***Al_2O_3	***ns***SiO_2-***ns***TiO_2	***ns***Al_2O_3-***ns***TiO_2	***ns***SiO_2-***ns***Al_2O_3-***ns***TiO_2
Conversion (%)	75.2	76.4	92.4	82.4
Cracked sel. (%)	88.4	87.4	97.7	92.1
Isoparaffin sel. (%)	71.7	72.6	69.8	70.0
Olefin sel. (%)	15.1	13.9	17.8	16.1
C_3~C_4 sel. (%)	19.9	19.4	16.2	21.0
C_5~C_{13} sel. (%)	68.5	68.0	81.5	71.1
C_{16} sel. (%)	11.6	12.6	2.3	7.9

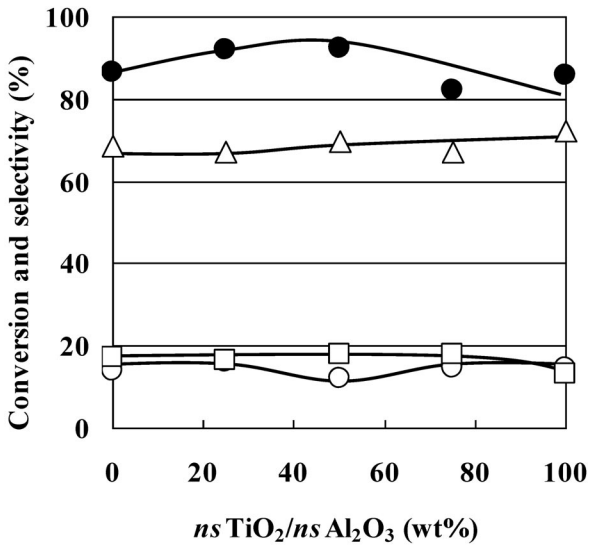

Fig. 10 Conversion and selectivity depending on the ***ns***TiO_2/***ns***Al_2O_3 ratio. ●: conversion; ○: normal paraffins; △: isoparaffins; □: olefins.

Catalytic performance depending on various reduction conditions

The performance of the tricomponent catalyst that has various states of Ni was investigated. The catalysts were prepared in three different ways. Supporting condition (1): reduction after composed with Ni and Mo were co-supported on γ-Al_2O_3, ***ns***Al_2O_3, and zeolite. Supporting condition (2): reduction after Ni and Mo were co-supported on γ-Al_2O_3, composed with ***ns***Al_2O_3 and zeolite. Supporting condition (3): supporting Ni on γ-Al_2O_3, and supporting Mo on reduced Ni/γ-Al_2O_3. Table 3 shows the catalyst performance depending on the preparation methods used: Supporting condition (3) had the highest isoparaffin selectivity and the lowest olefin selectivity. From these results, it is considered that the reduction states of Ni and Mo are different among the preparation methods. Therefore, the states of Ni and Mo were measured by XPS using the Ar-etching method.

Table 3 Catalyst performance depending on various preparation methods.

Supporting condition	(1)	(2)	(3)
Conversion (%)	86.6	86.8	88.6
Cracked sel. (%)	96.7	96.6	96.7
Isoparaffin sel. (%)	68.7	69.1	70.2
Olefin sel. (%)	17.1	15.3	14.3
C_3~C_4 sel. (%)	18.3	21.0	23.3
C_5~C_{13} sel. (%)	78.4	75.6	73.4
C_{16} sel. (%)	3.3	3.4	3.3

Supporting condition (1): reduction after composed with Ni and Mo were co-supported on γ-Al_2O_3, ***ns***Al_2O_3 and zeolite.
Supporting condition (2): reduction after Ni and Mo were co-supported on γ-Al_2O_3, composed with ***ns***Al_2O_3 and zeolite.
Supporting condition (3): supporting Ni on γ-Al_2O_3, and supporting Mo on reduced Ni/γ-Al_2O_3.

Characterization of the tricomponent catalyst by H_2-TPR and X-ray photoelectron spectroscopy

The reduction temperature of Ni was measured by H_2 temperature-programmed reduction. As shown in Fig. 11, the Ni/γ-Al_2O_3 catalyst and metal catalysts were measured. Ni/γ-Al_2O_3 catalyst has two peaks at 320 and 400~650 °C; the peak at the lower temperature shows that NiO is dispersed on γ-Al_2O_3, the peak at the higher temperature shows that NiO is tightly bound to γ-Al_2O_3. On the other hand, reduction temperature of the metal catalyst shifted to a higher temperature than that of the Ni/γ-Al_2O_3 catalyst. For example, the peak at the lower temperature shifted from 320 to 420 °C, another one shifted to over 700 °C. Thus, it is considered that reduction of NiO the metal catalyst is difficult because oxygen from MoO_3 is supplied to NiO.

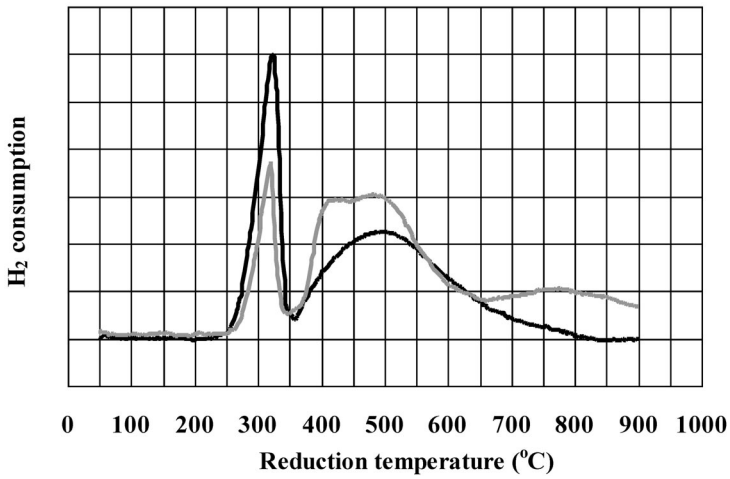

Fig. 11 H_2-TPR spectra of Ni or NiMo/γ-Al_2O_3 catalysts. Black line: Ni/γ-Al_2O_3; gray line: NiMo/γ-Al_2O_3.

The states of Ni and Mo were confirmed by XPS using the Ar-etching method (at depths of 5, 10, and 15 nm). The surface layer of the tricomponent catalyst after reduction was measured. Figure 12 shows a peak of Ni2p at a depth of 10 nm. The two peaks NiO and Ni were observed at a binding energy of 864 and 862 eV, respectively. The peak intensity of NiO was the highest in method 1, and the peak intensity of Ni was the highest in method 3. In addition, Fig. 13 shows a peak of Mo3d at a depth of 10 nm, and a peak of MoO_3 was observed at a binding energy of 237.5 eV. The peak intensity of MoO_3 was the lowest in method 1. NiO in method 3 is difficult to reduce by hydrogen because oxygen is supplied from MoO_3 to NiO. It is considered that the tricomponent catalyst can have higher performance by prior reduction of NiO.

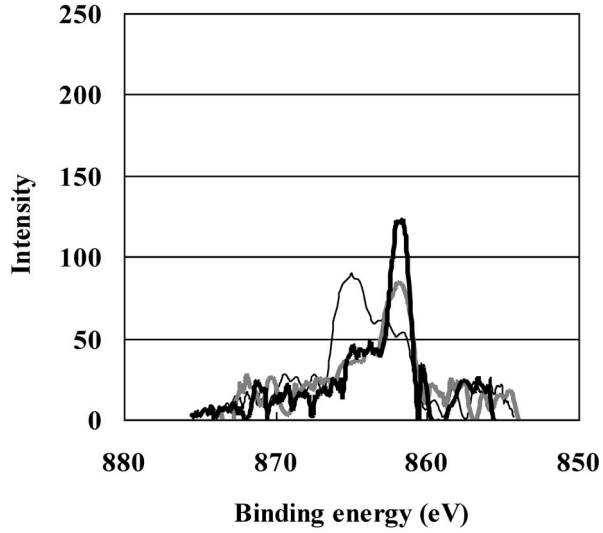

Fig. 12 Signal intensity of the Ni2p regions at a depth of 10 nm by XPS. Fine line: supporting condition (1); gray line: supporting condition (2); black line: supporting condition (3). Refer to footnote of Table 3.

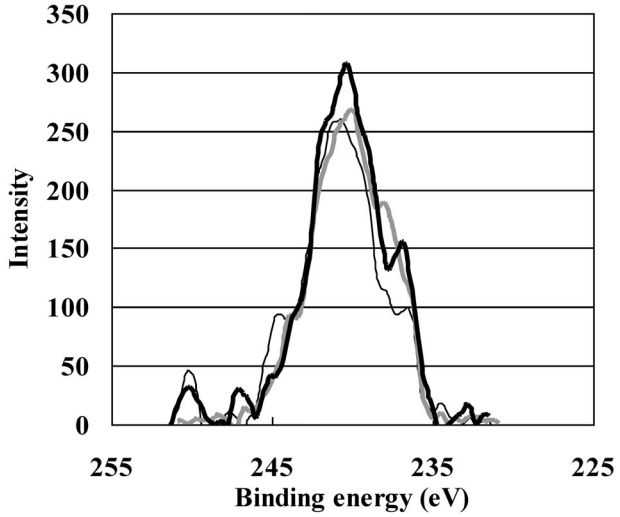

Fig. 13 Signal intensity of the Mo3d regions at a depth of 10 nm by XPS. Fine line: supporting condition (1); gray line: supporting condition (2); black line: supporting condition (3). Refer to footnote of Table 3.

CONCLUSION

The tricomponent catalyst consisting of NiMo/γ-Al_2O_3, ***ns***Al_2O_3, and H-beta zeolite has a relatively high selectivity for hydro-reforming large *n*-paraffins to lighter isoparaffins. The concerted effect of this catalyst can be increased to control the [NiMo/γ-Al_2O_3]/[H-beta zeolite] ratio and ***ns***Al_2O_3 content. In addition, ***ns***Al_2O_3-***ns***TiO_2 had the highest activity and cracking ability with an over-cracking suppression due to individual and concerted effect of ***ns***Al_2O_3 and ***ns***TiO_2. Higher catalytic performance can be obtained by changing the supporting condition of Ni and Mo by supporting Ni on γ-Al_2O_3, and supporting Mo on reduced Ni/γ-Al_2O_3.

ACKNOWLEDGMENTS

We gratefully acknowledge the financial support from CREST-JST (Japan Science and Technology Agency), the basic analyses performed by the Instrument Center of The University of Kitakyushu, and the assistance of our coworkers, M. Yoshino and S. Sudo.

REFERENCES

1. D. Li, T. Sato, M. Imamura, H. Shimada, A. Nishijima. *Appl. Catal., B* **16**, 255 (1998).
2. S. Hwang, J. Lee, S. Park, D. R. Park, J. C. Jung, S. B. Lee, I. K. Song. *Catal. Lett.* **129**, 163 (2009).
3. S. Hwang, J. Lee, J. G. Seo, D. R. Park, M. H. Youn, J. C. Jung, S. B. Lee, I. K. Song. *Catal. Lett.* **132**, 410 (2009).
4. V. M. Benitez, J. C. Yori, J. M. Grau, C. L. Pieck, C. R. Vera. *Ener. Fuel* **20**, 422 (2006).
5. A. Martínez, G. Prieto, M. A. Arribas, P. Concepción. *Appl. Catal., A* **309**, 224 (2006).
6. M. Busto, M. E. Lovato, C. R. Vera, K. Shimizu, J. M. Grau. *Appl. Catal., A* **355**, 123 (2009).
7. B. Qiu, X. Yi, L. Lin, W. Fang, H. Wan. *Catal. Commun.* **10**, 1296 (2009).
8. V. Calemma, S. Peratello, F. Stroppa, R. Giardino, C. Perego. *Ind. Eng. Chem. Res.* **43**, 934 (2004).
9. F. A. N. Fernandes, U. M. Teles. *Fuel Proc. Technol.* **88**, 207 (2007).
10. M. Mitsios, D. Guillaume, P. Galtier, D. Schweich. *Ind. Eng. Chem. Res.* **48**, 3284 (2009).
11. I. Rossetti, C. Gambaro, V. Calemma. *Chem. Eng. J.* **154**, 295 (2010).
12. V. Calemma, C. Gambaro, W. O. Parker Jr., R. Carbone, R. Giardino, P. Scorletti. *Catal. Today* **149**, 40 (2010).
13. D. Leckel, M. Liwanga-Ehumbu. *Ener. Fuel* **20**, 2330 (2006).
14. S. P. Elangovan, C. Bischof, M. Hartmann. *Catal. Lett.* **80**, 35 (2002).
15. J. F. M. Denayer, J. A. Martens, P. A. Jacobs, J. W. Thybaut, G. B. Marin, G. V. Baron. *Appl. Catal., A* **246**, 17 (2003).
16. C. S. Laxmi Narasimhan, J. W. Thybaut, G. B. Marin, J. F. Denayer, G. V. Baron, J. A. Martens, P. A. Jacobs. *Chem. Eng. Sci.* **59**, 4765 (2004).
17. J. C. Chavarria, J. Ramirez, H. Gonzalez, M. A. Baltanas. *Catal. Today* **98**, 235 (2004).
18. J. W. Thybaut, C. S. Laxmi Narasimhan, J. F. Denayer, G. V. Baron, P. A. Jacobs, J. A. Martens, G. B. Marin. *Ind. Eng. Chem. Res.* **44**, 5159 (2005).
19. G. Kinger, H. Vinek. *Appl. Catal., A* **218**, 139 (2001).
20. S. Zeng, J. Blanchard, M. Breysse, Y. Shi, X. Su, H. Nie, D. Li. *Appl. Catal., A* **294**, 59 (2005).
21. J. P. Giannetti, A. J. Perrotta. *Ind. Eng. Chem. Proc. Des. Dev.* **14**, 86 (1975).
22. W. S. Choi, K. H. Lee, K. Choi, B. H. Ha. *Stud. Surf. Sci. Catal.* **127**, 243 (1999).
23. B. C. Gagea, Y. Lorgouilloux, Y. Altintas, P. A. Jacobs, J. A. Martens. *J. Catal.* **265**, 99 (2009).
24. A. Chica, U. Diaz, V. Fornés, A. Corma. *Catal. Today* **147**, 179 (2009).
25. H. Kumar, G. F. Froment. *Ind. Eng. Chem. Res.* **46**, 4075 (2007).

26. C. Bouchy, G. Hastoy, E. Guillon, J. A. Martens. *Oil Gas Sci. Technol.* **64**, 91 (2009).
27. T. L. M. Maesen, S. Calero, M. Schenk, B. Smit. *J. Catal.* **221**, 241 (2004).
28. S. Asaoka, K. Ito, S. Minohara, M. A. Ali, H. S. Bamufleh. *Prepr. Pap.—Am. Chem. Soc., Div. Petr. Chem.* **50**, 372 (2006).
29. M. A. Ali, S. Asaoka. *Petr. Sci. Technol.* **27**, 984 (2009).
30. S. Asaoka, M. Miyazaki, S. Minohara, K. Sakashita. *Stud. Surf. Sci. Catal.* **172**, 613 (2007).
31. K. Sakashita, K. Ito, S. Asaoka. *Prepr. Pap.—Am. Chem. Soc., Div. Petr. Chem.* **53**, 1 (2008).
32. K. Ito, H. Jang, K. Sakashita, S. Asaoka. *Pure Appl. Chem.* **80**, 2273 (2008).
33. T. Kimura, K. Sakashita, X. Li, S. Asaoka. *Prepr. Pap.—Am. Chem. Soc., Div. Petr. Chem.* **56**, 65 (2011).
34. K. Sakashita, T. Kimura, M. Yoshino, S. Asaoka. *J. Jpn. Petrol. Inst.* **54**, 320 (2011).
35. T. Kimura, J. Gao, K. Sakashita, X. Li, S. Asaoka. *J. Jpn. Petrol. Inst.* **55**, 40 (2012).
36. T. Kimura, K. Sakashita, X. Li, S. Asaoka. *J. Jpn. Petrol. Inst.* **55**, 99 (2012).
37. T. Kimura, N. Hata, K. Sakashita, S. Asaoka. *Catal. Today* **185**, 119 (2012).
38. T. Kimura, K. Sakashita, X. Li, S. Asaoka. *Catal. Survey Asia* **15**, 259 (2011).
39. K. Sakashita, M. Yoshino, I. Nishimura, Y. Hayakawa, S. Asaoka. *Prepr. Pap.—Am. Chem. Soc., Div. Petr. Chem.* **54**, 38 (2009).
40. K. Sakashita, I. Nishimura, M. Yoshino, T. Kimura, S. Asaoka. *J. Jpn. Petrol. Inst.* **54**, 180 (2011).
41. K. Sakashita, I. Nishimura, T. Kimura, S. Asaoka. *J. Jpn. Petrol. Inst.* **54**, 248 (2011).
42. W. Suarez, J. A. Dumesic, C. G. Hill Jr. *J. Catal.* **94**, 408 (1985).

